NY10189 is being considered for publication in Physical Review Applied as a Research Article.

Abnormal defect physics of ternary semiconductor $ZnGeP_2$ with high density of anion-cation antisites: A first-principles study
by Menglin Huang, ShanShan Wang, Yu-Ning Wu, et al.

Dear Dr. Lambrecht,

We would appreciate your review of this manuscript, which has been submitted to Physical Review Applied. We append below the abstract of the manuscript. We realize that you may not be able to respond quickly, or at all, due to the current COVID-19 crisis. However, if you can, we would be grateful for your reply within 3 days, advising of your ability to return a report within 21 days. If you need extra time to prepare a report, or we can do something else to help you with your review, please let us know. If you cannot review, advice on suitable referees would be welcome.

To accept to review, visit:
https://referees.aps.org/reviews/NY10189-1e6851b-167976/promise

To decline to review, visit:
https://referees.aps.org/reviews/NY10189-1e6851b-167976/decline

If you need more information or would like to send us a report now, please log into our referee server at:
https://referees.aps.org/r/NY10189

Physical Review Applied is dedicated to publishing high-quality papers at the intersection of physics and engineering, among other disciplines. To be publishable as a Research Article, a manuscript should be at the level of a good regular article in one of the traditional Physical Review journals. It is important to us that the papers we publish be of interest to more than a small group of readers; have real implications and significance; have strong and clear ties to concrete applications; and offer fresh insight from or about physics.

Is the main achievement of this study obvious to you, and significant? Mere correctness is not sufficient justification for publication in our journal.

Should the authors be encouraged to add extra detail or results to this paper, to make it more informative and stronger? Are they

making full use of the available literature on this topic?

Is the emphasis sufficiently on physics and application, as opposed to materials science? Again, the ties should be strong and clear. Such deficiencies often can be cured by rewriting, or by including additional prose, without performing additional research.

Supplemental Material associated with this manuscript is available via our referee server.

Thank you for your help.

Yours sincerely,

Qiao Qiao
Associate Editor
Physical Review Applied
Email: prapplied@aps.org

ADDITIONAL MATERIAL AVAILABLE (SEE FULL REFERRAL LETTER):

- Supplemental Material intended for publication (via referee server)
- Memo: Advice to referees Physical Review Applied

Abnormal Defect Physics of Ternary Semiconductor $ZnGeP_2$ with High Density of Anion-Cation Antisites: a First-Principles Study

Menglin Huang[1#], ShanShan Wang[1#], Yu-Ning Wu[1*] and Shiyou Chen[1,2†]

[1]*Key Laboratory of Polar Materials and Devices (MOE), East China Normal University, Shanghai 200241, China*
[2]*State Key Laboratory of ASIC and System, School of Microelectronics, Fudan University, Shanghai 200433, China*
The authors contribute equally.
* ywu@phy.ecnu.edu.cn, † chensy@fudan.edu.cn

Abstract

The anion-cation antisite defects usually have low density in the group III-V (*e.g.*, GaN) and II-IV-V_2 ($ZnGeN_2$, $ZnSnP_2$) semiconductors and thus have not drawn enough attention in the defect study of $ZnGeP_2$ since 1976. However, our first-principles calculations based on hybrid functional show that the anion-cation antisite defects (Ge_P and P_{Ge}) can have very high density (10^{17}-10^{18} cm^{-3}), making them the dominant defects in $ZnGeP_2$. Their calculated photoluminescence (PL) spectra agree well with the 1.4 and 1.6 eV PL peaks observed experimentally, indicating that they may be the origin defects, which challenges the previous assumptions that the P vacancy (V_P) defect is responsible for the two PL peaks. Although the anion-cation antisites (Ge_P and P_{Ge}) and cation-cation antisites (Ge_{Zn} and Zn_{Ge}) both have density as high as 10^{17} cm^{-3}, $ZnGeP_2$ suffers serious donor-acceptor compensation, which results in low carrier density (below 10^{10} cm^{-3}) and thus poor electrical conductivity. These results explain the mysterious observation that $ZnGeP_2$ crystals grown using different methods have high defect density but low carrier density and high resistivity. Defect passivation and lower crystal growth temperature are proposed for suppressing the defect-induced optical absorption in the development of high-power $ZnGeP_2$-based optical devices.

I. Introduction

$ZnGeP_2$ is a group II-IV-V_2 semiconductor in the chalcopyrite structure, which can be derived from the binary zincblende-structured GaP via cation mutation, *i.e.*, replacing the group III cation Ga^{3+} by the group II Zn^{2+} and group IV Ge^{4+}. It is one of the most promising infrared nonlinear optical materials that can be used for frequency conversion, second harmonic generation (SHG) and optical parametric oscillator (OPO), owing to its large nonlinear optical coefficient, high thermal conductivity and sufficient birefringence [1-16].

In the development of high-power $ZnGeP_2$-based optical devices, the presence of point defects in the crystals is a serious limiting factor, *e.g.*, although the material is relatively transparent for the 0.7-2.5 μm light, there is still a broad defect-related absorption band [17-25]. It was reported that the density of both the donor and acceptor defects can be as high as 10^{19} cm^{-3} [26,27], indicating that the influences of point defects can be significant. Interestingly, despite a so high density of defects, the electrical conductivity of grown crystals is very poor. $ZnGeP_2$ crystal can be grown using Bridgman method [28-30] or high pressure physical vapor transport (HPVT) [19,31]. The Bridgman-grown $ZnGeP_2$ exhibits p-type conductivity with a low hole density 10^{10} cm^{-3} [32-34], whereas the HPVT-grown $ZnGeP_2$ was reported to show n-type conductivity with high resistivity [19,31].

To understand the origin of the broad defect-related absorption band and the high resistivity, both experimental and theoretical techniques have been adopted to study the point defects in $ZnGeP_2$ [19,35-41]. The photoluminescence (PL) spectra show that the Bridgman-grown p-type $ZnGeP_2$ exhibits three different PL peaks around 1.23 eV [35], 1.4 eV [23,36] and 1.6 eV [20,23,32,35,36,42], while the HPVT-grown crystals have the exclusive 1.2 eV emission [19,42]. The electron paramagnetic resonance (EPR) [17,18,22,43-45] had also been used to characterize the defects, which attributes both the 1.4 eV and 1.6 eV PL peaks to the P vacancy (V_P) defect [23,36], while the 1.2 eV defect to the antisite on cation sites [19]. Theoretically, Jiang *et al.* calculated the formation energies of five point defects V_{Zn}, V_{Ge}, Ge_{Zn}, Zn_{Ge} and V_P, trying to explain the PL peaks and EPR signals according to these defects, and found Ge_{Zn} has a low formation energy and can act as a p-type limiting defect [38-41].

Despite these pioneer studies, the defect physics in $ZnGeP_2$ has not yet been well understood. The early EPR study in 1976 had mentioned an anion-cation antisite defect, presumably the neutral P_{Ge} antisite [17,46]. Surprisingly, the anion-cation

antisite defects had neither been observed in a large number of experimental studies in the following decades [17-21,23,26,27,35-37], nor considered in the first-principles calculation study [38-41,47,48], so it is unclear whether these antisites exist or have high density in the grown $ZnGeP_2$ crystals. Most of the previous defect studies were focused on the point defects such as V_{Zn}, V_{Ge}, Ge_{Zn}, Zn_{Ge} and V_P. In fact, such kind of defects (vacancies and cation-cation antisites) are also the dominant defects in other II-IV-V_2 semiconductors such as $ZnGeN_2$, $ZnSnN_2$ and $ZnSnP_2$ [49-53], so it is natural to focus on these defects also in $ZnGeP_2$. However, an obvious difference should be noted between $ZnGeP_2$ and other II-IV-V_2 semiconductors, *i.e.*, $ZnGeP_2$ has high density of defects but also high resistivity, so the defects do not increase the electrical conductivity, in contrast to the cases in other II-IV-V_2 ($ZnSnN_2$, $ZnSnP_2$) semiconductors which are found to have metallic-like conductivity contributed by high density of defects [49,50,53-56]. This difference indicates that the defect physics may be quite different in $ZnGeP_2$.

In this paper, we revisit the defect physics of $ZnGeP_2$ through systematical first-principles calculations based on hybrid functional, and found that the defect physics of $ZnGeP_2$ is quite abnormal because very high density of cation-anion antisite defects (Ge_P and P_{Ge}) can form and become the dominant defects. The importance of these cation-anion antisites has been neglected since 1976, and deserves special attention in the future defect characterization studies. Furthermore, the high density of antisite defects, including the donor defects Ge_P and Ge_{Zn} and acceptor defects P_{Ge} and Zn_{Ge}, induce serious donor-acceptor compensation, resulting in a low hole carrier density and thus high resistivity. The calculated PL spectra of these defects show that the PL peaks around 1.4 eV and 1.6 eV may originate from Ge_P and P_{Ge} and the 1.2 eV peak from Ge_{Zn}, which challenges the previous opinions that the P vacancies are responsible for the two PL peaks at 1.4 and 1.6 eV.

II. Calculation Methods

A. Defect Formation Energies

All the structural relaxation and total energy calculations are performed based on the density functional theory and using the plane-wave pseudopotential methods as implemented in the Vienna ab initio simulation package (VASP) [57]. For the exchange-correlation functional, the hybrid functional in the Heyd-Scuseria-Ernzerhof

(HSE) [58,59] form is adopted with the standard exchange parameter α=0.25 and screening parameter μ=0.2 $Å^{-1}$. The projector augmented wave (PAW) [60,61] pseudopotentials are used and Zn $3d^{10}$ $4s^2$, Ge $4s^2$ $4p^2$ and P $3s^2$ $3p^3$ electrons are treated as valence electrons. The cutoff energy of the planewave basis is set to 350 eV, and a 6×6×3 Monkhorst k-point mesh [62] is used for the primitive cell and single Γ point for the 144-atom defect supercell. The convergence test with larger supercell and denser k-point meshes showed that the results are converged.

The formation energy of the point defect α in the ionized charge state q is calculated by [63,64],

$$\Delta H_f(\alpha, q) = E(\alpha, q) - E(ZnGeP_2) + \sum n_i(E_i + \mu_i) + q(E_F + E_{VBM} + \Delta V) \quad (1)$$

where $E(\alpha, q)$ is the total energy of the supercell with a defect α in its charge state q, and $E(ZnGeP_2)$ is the total energy of the pure $ZnGeP_2$ supercell. μ_i is the atomic chemical potential of an atom reservoir of the element *i*, referenced to the energy E_i of the pure elemental phases of Zn, Ge and P. E_{VBM} is the eigenvalue of valence band maximum (VBM) state in bulk supercell and E_F is the Fermi energy referenced to the VBM level. ΔV aligns the averaged electrostatic potential of the farthest area from the defect in the supercell. Image charge correction caused by finite supercell size is also added for charged defects [65,66].

B. Defect and Carrier Densities

For a defect α in its charge state q, the equilibrium density $n(\alpha, q)$ is a function of its formation energy, which can be given by [63,64],

$$n(\alpha, q) = N_{sites} g_q e^{\frac{-\Delta H_f(\alpha,q)}{k_B T}} \quad (2),$$

where $\Delta H_f(\alpha, q)$ is the defect formation energy, k_B is the Boltzmann constant, T is the temperature. N_{sites} is the number of defect sites per unit volume, and g_q is the degeneracy factor which reflects the number of possible configurations for electrons occupying the defect level and changes with charge state q.

Since the ionized defects produce carriers and become charged, we can calculate the charge density of all the ionized acceptor defects (N_A^-) and the charge density of all the ionized donor defects (N_D^+). For non-degenerate semiconductors, the density of hole and electron carriers follows the Boltzmann distribution, which is given by,

$$p_0 = N_v e^{-E_F/k_B T} \quad (3),$$

$$n_0 = N_c e^{(E_F - E_g)/k_B T} \quad (4),$$

where N_v and N_c are the effective density of states for valence band and conduction band edges. N_A^-, N_D^+, n_0 and p_0 should satisfy the charge neutrality condition,

$$p_0 + N_D^+ = n_0 + N_A^- \quad (5).$$

By solving this equation self-consistently, we can determine the Fermi level E_F, electron and hole carrier density, and the density of all point defects in different charge states under different chemical potential (growth) conditions [67,68].

Since the crystals are usually grown at a high growth temperature and then annealed to room temperature, the defects form during the growth and may change their charge states after the annealing which can change the Fermi level and carrier density. Therefore, we first solve the equation at high growth temperature and determine the density of all point defects in different charge states, then we solve the equation again at the room temperature. At room temperature, we fix the summed density of different charge states for each defect and determine the density of different charge states according to the Fermi-Dirac distribution of the electrons on the defect levels, then a redistributed density of defects in different charge states, carrier density and Fermi level can be calculated [64,69,70].

C. Photoluminescence Spectrum

The photoluminescence spectrum of the defect states can be calculated according to spectral function [71,72],

$$\mathrm{A}(\hbar\omega) = \omega^3 \sum_m p_m \sum_n \left|\langle \chi_{im} | \chi_{fn} \rangle\right|^2 \delta(E_{ZPL} + E_{im} - E_{fn} - \hbar\omega) \quad (6)$$

where p_m is the Boltzmann factor, which reflects the thermal occupation of the initial vibrational state m. $\langle \chi_{im} | \chi_{fn} \rangle$ is the overlap integral between initial and final vibrational wavefunctions, which can be approximated by some analytical forms [73]. Here we use finite-difference method to solve the time-independent one-dimensional (1D) Schrödinger equation along the 1D harmonic potential surface both for initial and final states, and then wavefunctions can be used to numerically calculate the overlap integral. E_{ZPL} is the zero phonon line, which corresponds to the charge-state transition energy level of defects.

III. Results and Discussion

A. Phase Stability

In order to calculate the formation energies of defects according to Eq. (1), we need to determine the chemical potentials of Zn, Ge and P that can stabilizes the ternary compound $ZnGeP_2$, so we need to study its phase stability first. $ZnGeP_2$ has a tetragonal chalcopyrite structure with the space group of I-42d, which can be derived from the zinc-blende structure by occupying the cation sites with Zn and Ge orderly (shown in Fig. 1a). Our HSE calculated lattice constants, a = 5.468 Å and c= 10.745 Å, are highly consistent with experimental values as shown in Table I. In contrast, the semi-local functional GGA [74] overestimates while LDA [75] underestimates the lattice constants. With the HSE optimized structure, the band gap of $ZnGeP_2$ is found to be 2.058 eV at Γ point, which also agrees well with the experimental values (2.0-2.1 eV) [22,76,77] and a recent HSE calculated value of 2.15 eV [78].

Table I. The calculated lattice constants of $ZnGeP_2$, compared with the experimental and previous calculated results.

	a (Å)	c (Å)	η=c/2a
This work	5.468	10.745	0.983
Experiments	5.46 [28]	10.71 [28]	0.981
	5.466 [79]	10.722 [79]	0.981
	5.465 [80]	10.771 [80]	0.985
Calculations	5.499 [81]	10.840 [81]	0.986 (GGA)
	5.396 [82]	10.665 [82]	0.988 (LDA)
	5.473 [83]	10.749 [83]	0.982 (HSE)

To predict whether this ternary compound $ZnGeP_2$ is stable relative to the competing phases that can be formed by Zn, Ge and P, the range of their chemical potential μ_i (i=Zn, Ge or P) that stabilizes $ZnGeP_2$ is calculated. Under the thermodynamic equilibrium, the chemical potentials of Zn, Ge and P should satisfy,

$$\mu_{Zn} + \mu_{Ge} + 2\mu_P = \Delta H_f(ZnGeP_2) = -0.98\, eV,$$

where $\Delta H_f(ZnGeP_2) = -0.98\, eV$ is the calculated formation enthalpy of $ZnGeP_2$, slightly larger than the GGA calculated -0.89 eV[84]. Because μ_i=0 means the element is so rich that its pure elemental phase can form, so $\mu_{Zn} < 0$, $\mu_{Ge} < 0$ and $\mu_P < 0$ should also be satisfied in order to assure that no elemental phases of Zn, Ge or P coexist in the synthesized samples. In order to avoid the coexistence of secondary phases such as Zn_3P_2 and ZnP_2, the chemical potentials should also satisfy,

,

.

Based on the above equations and inequations, we can determine the chemical potential region that stabilizes pure $ZnGeP_2$, which is plotted in Fig. 1b (in 3-dimensional (μ_{Zn}, μ_{Ge}, μ_P) space) and Fig.1c (projected on the 2-dimensional (μ_{Zn}, μ_{Ge}) plane). The region with gradient color in Fig. 1b shows the stable chemical potential range of $ZnGeP_2$, which can also be projected on the 2-dimensional (μ_{Zn}, μ_{Ge}) plane in Fig. 1c. As we can see, as μ_{Ge} becomes lower and thus Ge becomes poorer in the synthesis condition, Zn_3P_2 and ZnP_2 will form. Therefore, μ_{Ge} is restricted in a small range near 0, which means the Ge-rich condition should always be satisfied for synthesizing pure $ZnGeP_2$ samples.

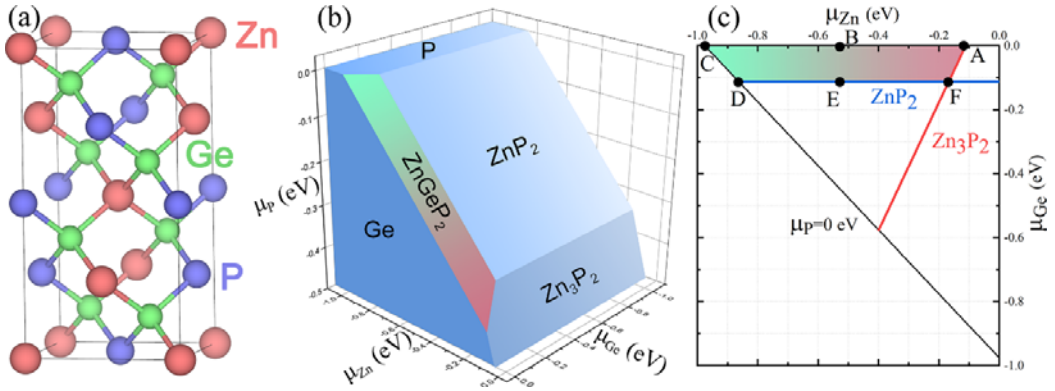

Figure 1. (a) The unit cell of chalcopyrite $ZnGeP_2$ crystal structure. (b) Thermodynamic chemical potential region (shown in gradient color) stabilizing $ZnGeP_2$ with respect to the competing secondary phases such as Zn, Ge, P, ZnP_2 and Zn_3P_2 in 3-dimensional (μ_{Zn}, μ_{Ge}, μ_P) space, and (c) the projection of chemical potential region on the (μ_{Zn}, μ_{Ge}) plane. Six points A, B, C, D, E, F are selected as the synthesis conditions under which the defect properties will be calculated.

It should be noted that the stable chemical potential range of $ZnGeP_2$ had also been calculated by Jiang *et al.* [38,39], however, their results differ significantly from ours. We attribute the difference to three reasons: i) they did not consider an important secondary phase ZnP_2, which can limit the stable chemical potential region significantly; ii) they considered a secondary phase GeP which, however, is found to be intrinsically unstable with a positive formation enthalpy according to our hybrid functional calculations and thus do not influence the chemical potential region, iii) they used the semi-local LDA functional but we use the hybrid functional. Our results

are also consistent with the recent X-ray photoelectron spectroscopy (XPS) result that the impurity phases during $ZnGeP_2$ growth are Zn_3P_2 and ZnP_2 [85].

B. Dominant Point Defects

After determining the stable chemical potential region of $ZnGeP_2$, we select six representative points in the region, and calculate the defect properties in the $ZnGeP_2$ samples synthesized under these conditions. In Fig. 2, the formation energies of all point defects (including three vacancies V_{Zn}, V_{Ge}, V_P, six antisites Zn_{Ge}, Zn_P, Ge_{Zn}, Ge_P, P_{Zn}, P_{Ge}, three interstitials Zn_i, Ge_i, P_i) in different charge states are plotted as functions of the Fermi level. For three interstitials, we considered at least 30 interstitial sites and showed only the results of the lowest-energy sites.

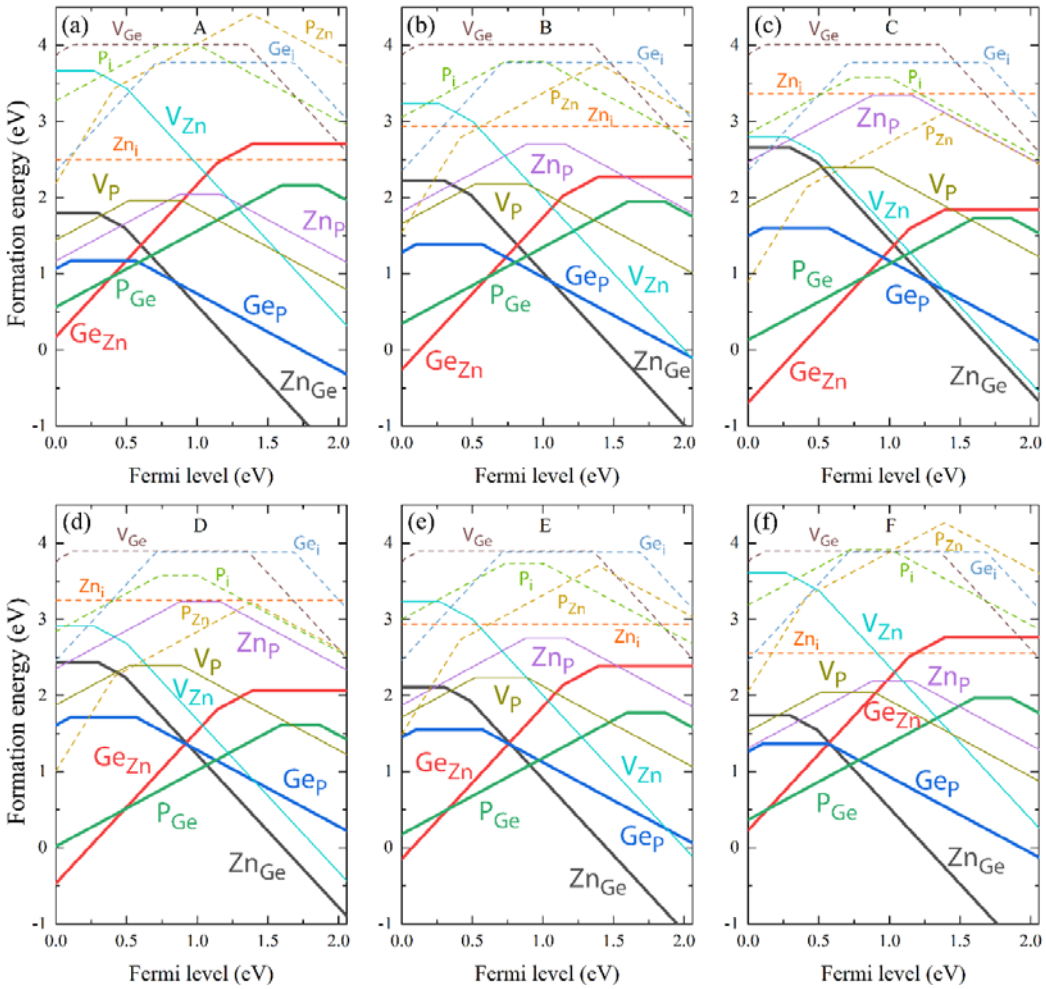

Figure 2. The calculated formation energies of point defects in different charge states

as a function of Fermi level under (a) Zn-rich, Ge-rich (b) Zn-moderate, Ge-rich (c) Zn-poor, Ge-rich (d) Zn-poor, Ge-poor (e) Zn-moderate, Ge-poor and (f) Zn-rich, Ge-poor condition.

Among the defects, V_{Ge}, P_{Zn} and all the interstitial defects have too high formation energies (always higher than 1 eV, as shown by the dashed lines), so they have negligible density in the synthesized samples and are thus unimportant. Four antisite defects, including two cation-anion antisites Ge_P and P_{Ge} and two cation-cation antisites Ge_{Zn} and Zn_{Ge}, are found to be the dominant defects with low formation energies under the six representative synthesis conditions. Ge_{Zn} and P_{Ge} are donor defects and have the lowest formation energies in the p-types samples with the Fermi level close to the VBM level, while Zn_{Ge} and Ge_P are acceptor defects and have the lowest formation energies in the n-type samples with the Fermi level close to the conduction band minimum (CBM) level. Therefore, they should have important influences on the electrical and optical properties of $ZnGeP_2$. We will now discuss their properties individually.

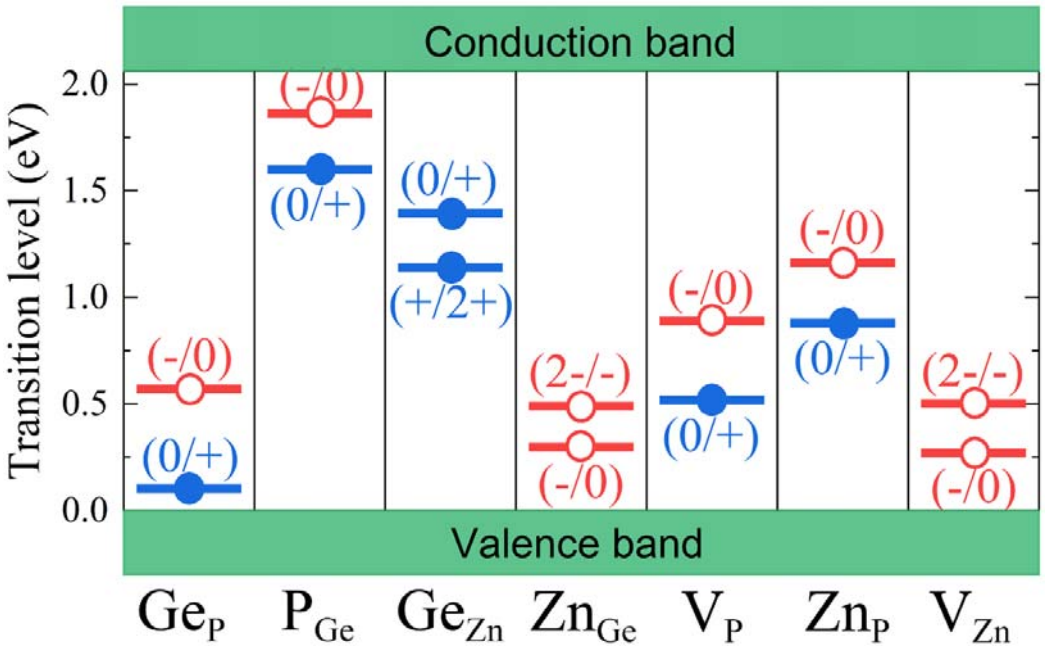

Figure 3. The calculated charge-state transition levels of point defects in the band gap of $ZnGeP_2$.

Ge_{Zn} acts as a deep donor with its (0/+) and (+/2+) transition energy levels located at 0.66 eV and 0.92 eV below the CBM level, as shown in Fig. 3. It is in the +1 and +2 charge states when Fermi level ranges from 0 to 1.39 eV, indicating that it becomes electrically active and contributes to n-type conductivity in this Fermi level range. Setzler *et al.* [17,18] observed the existence of singly ionized Ge_{Zn} (+1 charge state) using EPR, in consistent with our calculated low formation energy and high density of Ge_{Zn} in p-type samples. However, according to our calculated results, the formation energy of Ge_{Zn}^{2+} is much lower than that of Ge_{Zn}^{+} when Fermi level is low, so we predict that higher density of Ge_{Zn}^{2+} should also exist in the p-type $ZnGeP_2$. Very large atomic relaxation around Ge_{Zn} is found when the charge state changes from the neutral (0) state to the ionized +1 and +2 states. The four neighboring P atoms undergo an inward relaxation by 4.1% and 6.9% in 1+ and 2+ charge state, respectively. The deep nature of the Ge_{Zn} (0/+) and (+/2+) donor states and the large structural relaxation during ionization can be understood according to the electronic component analysis of the donor states. In Fig. 4a, we plot the norm squared wavefunction of the donor state. Obviously, the wavefunction is mainly localized on Ge cation and its neighboring P anions, which is the antibonding state of Ge 4s and P 3p hybridization. Because Ge 4s orbital level is much lower than the Zn 3s level, the donor level is low and deep in the band gap. In the neutral state, the antibonding donor level is occupied, so the Ge-P bond lengths are large, however, the level becomes partially occupied when the defect is ionized into the +1 state and fully unoccupied when it is ionized into the +2 state, so the Ge-P bonds shorten significantly.

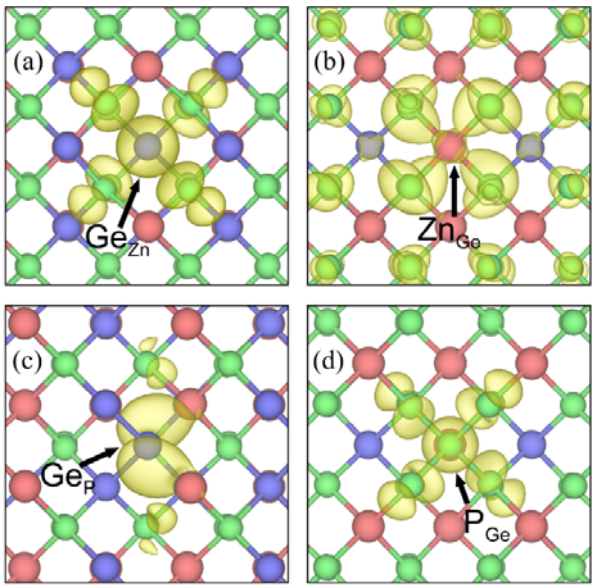

Figure 4. The norm-squared wavefunction of the defect eigenstates produced by (a) Ge_{Zn}, (b) Zn_{Ge}, (c) Ge_P and (d) P_{Ge}. The same colors are used as those in Fig.1 for Zn, Ge and P atoms.

In contrast to Ge_{Zn}, Zn_{Ge} is an acceptor with relatively shallow (-/0) and (2-/-) transition energy levels, located at 0.30 eV and 0.49 eV above VBM level. When Fermi level is close to CBM, the ionized Zn_{Ge}^{2-} can have very low formation energy and high density, which can limit the n-type conductivity. The atomic relaxation during the Zn_{Ge} ionization is rather small, *i.e.*, the corresponding Zn-P bonds in Zn_{Ge} 1- and 2- state remains almost unchanged. Since the Zn_{Ge} (-/0) and (2-/-) acceptor levels are relatively shallow, the wavefunction of the acceptor state is more delocalized, as shown in Fig. 4b, and the state is mainly composed of the P 3p orbitals.

P_{Ge} is a donor in a wide range of the Fermi level but becomes an acceptor when Fermi level is close to CBM. It has the (0/+) transition energy level at 0.46 eV below CBM, and (-/0) level at 0.20 eV below CBM. Fig. 4d shows the wavefunction of the P_{Ge} (0/+) donor level. Interestingly, the wavefunction is very similar to that of Ge_{Zn} donor level and localized mainly around the antisite P and surrounding P atoms, which indicates that the donor state is the antibonding state of the hybridization between P 3s and the surrounding P 3p orbitals. The donor level of P_{Ge} is higher in energy than that of Ge_{Zn}. The reason is double-folded, (i) the P 3s orbital energy is

higher than the Ge 4s orbital energy, (ii) the P-P bond around P_{Ge} is shorter than the Ge-P bond around Ge_{Zn} by 11.5% in the neutral state and by 10.0% in +1 charge state, indicating the P-P s-p hybridization around P_{Ge} is stronger than the Ge-P s-p hybridization around Ge_{Zn} and thus pushes the anti-bonding donor level upward.

Ge_P is the opposite of P_{Ge}, which acts as an acceptor in a wide range of Fermi level and becomes a donor only when the Fermi level is very low and close to the VBM level. The wavefunction in Fig. 4c shows that the Ge_P (-/0) acceptor state is quite different from other defect states, *i.e.*, although it is localized around the defect site, it has little hybridization contribution from the surrounding Ge around the antisite Ge. The state is mainly the Ge 4p orbital, and has a little contribution from the second-nearest-neighbor P 3p orbitals. Since the hybridization with the neighboring atoms is very weak, Ge_P (-/0) acceptor state can be viewed as a non-bonding state of Ge 4p orbital.

C. Defect and Carrier Density

Fig. 5 plots the calculated density of all defects in different charge states, Fermi energy and hole carrier density changing with the chemical potential points from A to F. Obviously, the four antisite defects in different charge states have much higher density (as high as 10^{17}-10^{18} cm^{-3}) than other defects, indicating that they are indeed the dominant defects in this ternary compound $ZnGeP_2$. Besides the four antisites, V_P, V_{Zn} and Zn_P can also have a density higher than 10^{14} cm^{-3}, so they may also have important influences on the electrical and optical properties of $ZnGeP_2$.

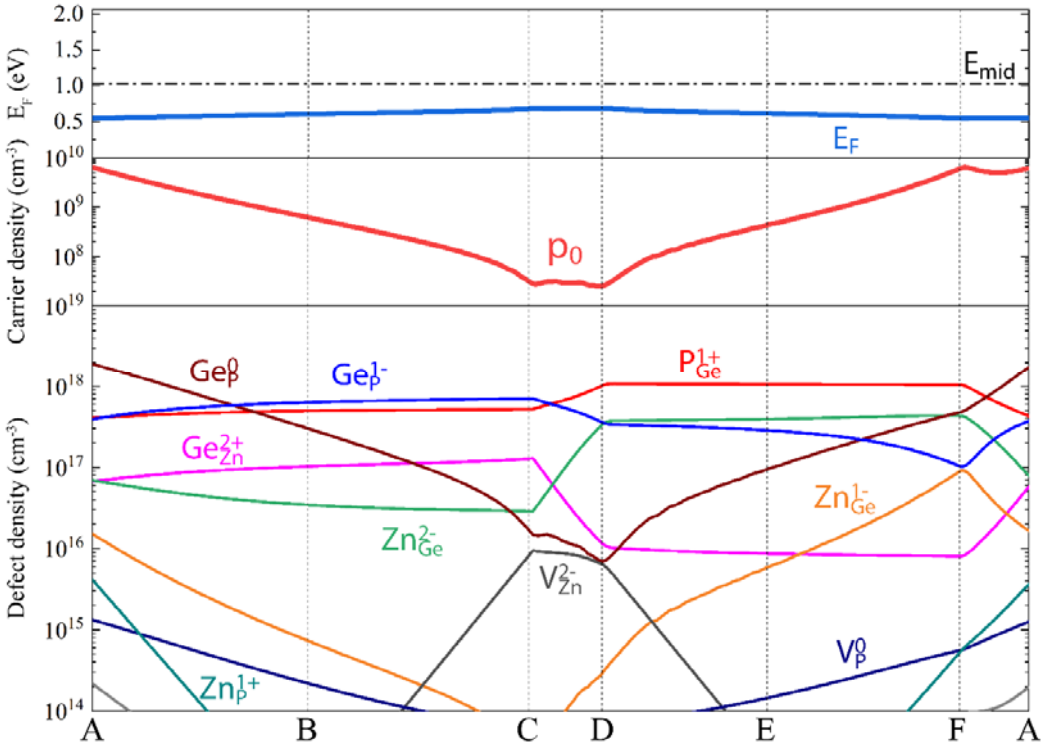

Figure 5. Calculated density of all defects, Fermi level and hole carrier density at room temperature (300 K) in the $ZnGeP_2$ crystals grown at a high temperature 1300 K and under different chemical conditions (corresponding to the chemical potential points from A to F in Fig. 1). Since the allowed range of is narrow in Fig. 1, its influence on the results are small and the Zn-rich (Zn-poor) condition are corresponding to P-poor (P-rich) condition.

One abnormal character of $ZnGeP_2$ defect properties is the high density of the anion-cation antisite defects Ge_P and P_{Ge}. In conventional III-V and II-VI semiconductors such as GaAs [86], GaN [87], InP [88] or ZnO [89], the anion-cation antisite defects usually do not exist, *i.e.*, the density is negligible. Furthermore, in other II-IV-V_2 ternary compounds such as $ZnSnN_2$ [49,50], $ZnGeN_2$ [51,52] and $ZnSnP_2$ [53] that have been studied in the past decade, the anion-cation antisite defects have never been reported to have a high density (Zn-Sn and Zn-Ge antisites are found to be the only dominant defects in $ZnSnN_2$, $ZnGeN_2$ and $ZnSnP_2$, but Sn-N, Ge-N or Sn-P antisites have not been reported). However, our calculations showed that Ge_P and P_{Ge} can have high density in the chalcopyrite-structured $ZnGeP_2$. The origin can be attributed to the small atomic size difference and the small electronegativity difference between Ge and P, compared to those of Sn-N, Sn-P and

Ge-N. It should be noted that the anion-cation antisite defects Ge_P and P_{Ge} had not been considered by Jiang *et al.* in their calculation study on the defect properties of $ZnGeP_2$ [38,39], so their high density had never been reported.

Although the acceptor defect Ge_P and donor defect P_{Ge} have high density in $ZnGeP_2$, their compensation limits the carrier density and the electrical conductivity to a low level. As shown in Fig. 2 and Fig. 5, the compensation between Ge_P^- and P_{Ge}^+ pins the Fermi level at 0.55 eV under Zn-rich condition and 0.69 eV under Zn-poor condition, so the corresponding hole carrier density is always low, only 6.4×10^9 and 2.5×10^7 cm^{-3}, respectively. Under Zn-rich condition (point A), the calculated hole density 6.4×10^9 cm^{-3} is in good agreement with the experimentally measured value about 10^{10} cm^{-3} in p-type $ZnGeP_2$ [32]. Under Zn-poor/Ge-poor condition, the hole density becomes even lower, which also agrees with the high resistivity observed in $ZnGeP_2$ grown by HPVT [19]. Experimentally, the HPVT samples were reported to be n-type but with high resistivity [19], however, our calculated very low carrier density and the Fermi level at the middle of the band gap show that the HPVT samples are actually intrinsic (rather than n-type, just more n-type and less p-type than the Bridgman-grown samples) and thus have high resistivity. The experiments had also shown that the density of both the donor and acceptor defects are around 10^{19} cm^{-3} [26,27], which are close to our calculated density of the dominant donor defect P_{Ge} and the dominant acceptor defect Ge_P. Both our calculations and previous experiments showed high density of donor and acceptor defects while low density of hole carriers, confirming that there is serious donor-acceptor compensation in $ZnGeP_2$.

Despite the predicted high density, four of the dominant defects in the ionized charge states, *e.g.*, Ge_P^-, P_{Ge}^+, Ge_{Zn}^{2+} and Zn_{Ge}^{2-}, have not been identified by experiments. We think this is because the characterization of defects in $ZnGeP_2$ was mostly through EPR in the past decades, but for the four charged defects, the defect levels are always fully occupied or empty (full-shell state), which do not have unpaired electrons and thus cannot be observed by EPR. Therefore, the EPR characterization reported only P_{Ge}^0, Ge_{Zn}^+ and Zn_{Ge}^- [17,28,46], which have lower density than Ge_P^-, P_{Ge}^+, Ge_{Zn}^{2+} and Zn_{Ge}^{2-} according to our calculation in Fig. 5. Considering the much higher density of ionized defects that had not been observed in EPR characterization, we call for the characterization study of defects in $ZnGeP_2$

using other techniques.

D. Defect Origin of Photoluminescence Peaks

A series of experiments have shown that the p-type Bridgman-grown $ZnGeP_2$ have PL peaks at around 1.23 eV [35], 1.4 eV [23,36] and 1.6 eV [20,23,36], while the HPVT-grown samples only have the 1.2 eV peak [19]. In literature the 1.4 and 1.6 eV peaks were both attributed to the defect V_P [23,36] while the 1.2 eV defect was attributed to the antisite defect on cation site[19]. According to our calculated defect density, V_P has much lower density than the four dominant antisite defects Ge_{Zn}, Zn_{Ge}, Ge_P and P_{Ge}. It is thus natural to ask if the four antisites produce any PL peaks and if they are responsible for the three peaks observed experimentally.

Since the Fermi level is located at 0.55-0.69 eV above VBM, V_P, Ge_P and Zn_{Ge} are in the neutral and negative charge states, so their defect levels are occupied by electrons (Fig. 6b), which can be excited to the CBM level and produce photoluminescence when the excited electron on the CBM level has a radiative transition back to the defect level. The defect levels of V_P, Ge_P and Zn_{Ge} are 1.2-2 eV lower than the CBM level, so their emission can be possible origin of the 1.2, 1.4 and 1.6 eV PL peaks. The levels of Ge_{Zn} and P_{Ge} are high (1.2-1.8 eV above VBM), so they are unoccupied (Fig. 6b) and the two defects are in the positive charge states. Under photon illumination, the electrons on the VBM level can be excited to these high levels, then a hole is produced at the VBM level and the defect Ge_{Zn} (P_{Ge}) changes its charge state from positive to neutral. The radiative transition from the defect level to the VBM level can give rise to emissions in the range 1.2-1.8 eV, so they can also be possible origin of the 1.2, 1.4 and 1.6 eV PL peaks.

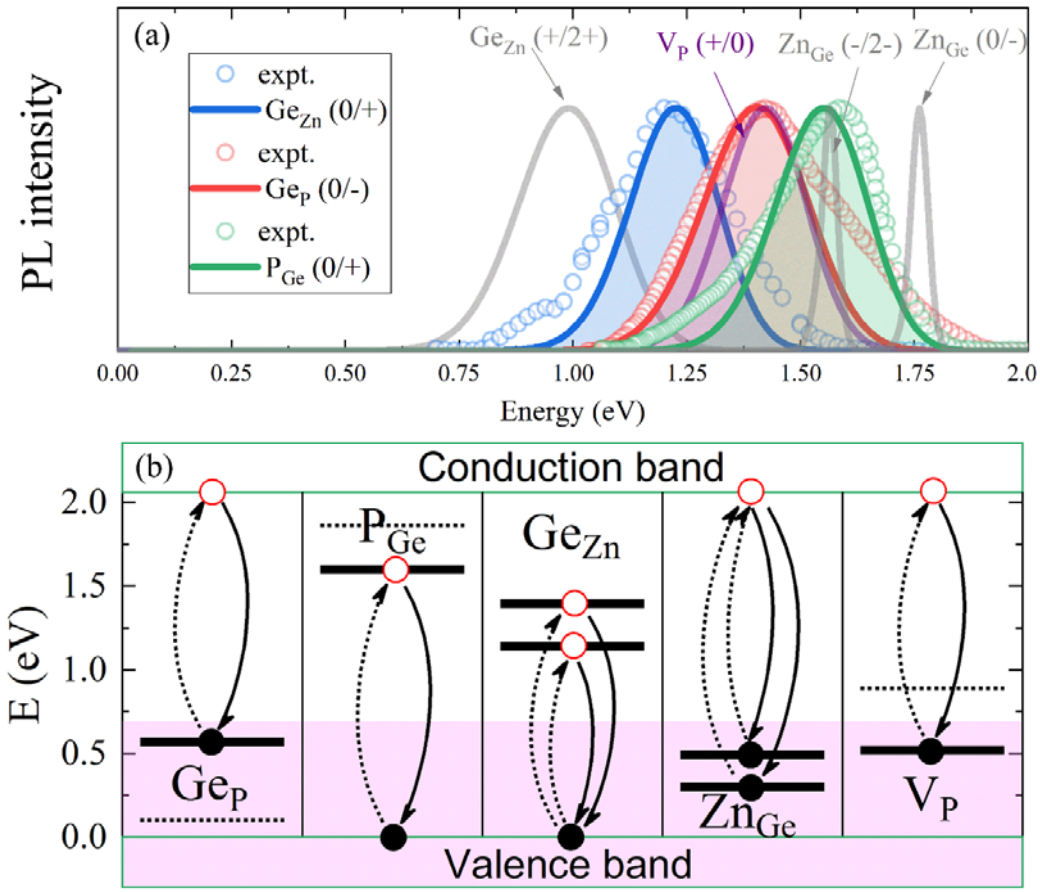

Figure 6. (a) Calculated photoluminescence spectrum of Ge_P, P_{Ge}, Zn_{Ge}, Ge_{Zn} and V_P in comparison with the experimental data extracted from Ref. [19,23,36]. The solid lines are the calculated results and the dots are the experimental values. (b) The corresponding schematic band diagram of carrier excitation and recombination processes. The Fermi level is set to 0.69 eV with the shaded pink area.

In Fig. 6a we show the calculated PL spectra of the possible origin defects according to the spectral function [72], and the critical factors influencing the spectra are shown in Table I. In the Supplementary material, we also show the detailed one-dimensional configuration coordinate diagram for each defect, which illustrates the corresponding electron excitation and recombination processes. Interestingly, the PL spectra of three defects, Ge_{Zn}, Ge_P and P_{Ge}, are highly consistent with the line shape of the experimental spectra.

Table I. The calculated factors that determine the PL spectra according to the

one-dimensional configuration coordinate diagram. ΔQ: mass-weighted structural difference in generalized coordinate. $E_{emission}$: emission energy that corresponds to the PL peak. $\hbar\Omega_g$: effective ground state vibrational energy fitted by our first-principles calculation data. E_{rel}: lattice relaxation energy. S_g: ground state Huang-Rhys factor.

Defect	ΔQ ($amu^{1/2}$ Å)	$E_{emission}$ (eV)	$\hbar\Omega_g$ (meV)	E_{rel} (eV)	S_g
Ge_{Zn} (0/+)	1.48	1.23	26.79	0.154	5.74
Ge_{Zn} (+/2+)	1.28	0.98	29.42	0.159	5.42
Ge_P (0/-)	1.72	1.37	22.08	0.174	7.87
P_{Ge} (0/+)	1.19	1.55	31.15	0.125	4.01
V_P (+/0)	2.64	1.40	14.55	0.141	9.69
Zn_{Ge} (0/-)	0.34	1.76	23.95	0.004	0.15
Zn_{Ge} (-/2-)	0.42	1.56	18.19	0.007	0.37

For Ge_P, the photoexcitation changes its state from Ge_P^- to Ge_P^0 (with an electron on the CBM level), and then the transition from Ge_P^0 to Ge_P^- gives rise to a PL peak at 1.37 eV, so it can be origin of the 1.4 eV PL peak observed experimentally [23,36]. For P_{Ge}, the photoexcitation changes its state from P_{Ge}^+ to P_{Ge}^0 (with a hole on the VBM level), and the transition from P_{Ge}^0 to P_{Ge}^+ gives rise to a PL peak at 1.55 eV, which can be origin of the observed 1.6 eV PL peak [20,23,36]. The calculated PL line shape of these two defects both agrees well with the measured PL spectra. Especially, both experiments and calculations show the 1.37 eV emission has a broader band than the 1.55 eV emission, which can be ascribed to the stronger electron-phonon coupling as reflected by the larger Huang-Rhys factors (see Table I). For Ge_{Zn}, the ground state is the positive charge state Ge_{Zn}^+ and the photoexcited state is Ge_{Zn}^0 with a hole on the VBM level. The transition from Ge_{Zn}^0 to Ge_{Zn}^+ gives rise to a 1.23 eV PL peak, which can be the origin of the PL peak at 1.2 eV [19].

The attribution of PL origin to the antisite Zn_{Ge} can be easily ruled out because either (0/-) or (-/2-) transition shows the very narrow PL shape, in contrast to the experimental one. This is in accordance with the small Huang-Rhys factors (weak electron-phonon coupling) shown in Table I. V_P was the previously assumed defect source of the PL peaks at 1.4 and 1.6 eV. Our calculation also indicates it has the

similar emission energy of 1.40 eV and large electron-phonon coupling. However, according to Fig. 6a, V_P shows a narrower PL than Ge_P, and the shape of Ge_P fits the experiment more. The smaller full width at half maximum (FWHM) of V_P PL can be ascribed to its smaller effective vibrational energy $\hbar\Omega_g$, leading to smaller vibrational wavefunction overlap. Considering the higher density of Ge_P than V_P, it is reasonable to attribute the origin of 1.4 eV PL peak to Ge_P, instead of the previously assumed V_P.

The appearance of the defect-induced PL peaks indicates that the defects can also induce obvious optical absorption in the energy range 1-2 eV, which can limit the transparence and thus the development of high-power optical devices such as OPO and SHG devices. Since the density of these origin defects is high and cannot be diminished to a low level at a high growth temperature 1300 K through changing the chemical potential conditions as shown in Fig. 5, the passivation of these defect levels in the band gap or the lowering of the crystal growth temperature become necessary, which should be paid special attention in the future development of high-power $ZnGeP_2$-based optical devices.

IV. Conclusions

Using the first-principles calculations based on the hybrid functional, we found that the defect physics of $ZnGeP_2$ is quite abnormal relative to other group II-IV-V_2 semiconductors. The anion-cation antisite defects, Ge_P and P_{Ge}, have unexpectedly high density and become the dominant defects in $ZnGeP_2$. However, their importance had been neglected in the long-term study on the defects in $ZnGeP_2$ after P_{Ge} was initially discussed in 1976. The calculated PL spectra of Ge_P and P_{Ge} agree well with the experimentally observed PL peaks at 1.4 eV and 1.6 eV, respectively, indicating that they may be origin defects of these two PL peaks, which challenges the previous assumptions that V_P is the origin of the two peaks in PL and EPR characterization studies. Both the cation-cation (Ge_{Zn}, Zn_{Ge}) and cation-anion (Ge_P, P_{Ge}) antisites are found to have high density, but P_{Ge} and Ge_{Zn} are donors while Ge_P and Zn_{Ge} are acceptors, so they cause serious donor-acceptor compensation, which results in a low carrier density and makes the Fermi level 0.55-0.69 eV above VBM. The serious donor-acceptor compensation explains the experimentally observed coexistence of

both high density of point defects and high resistance. According to these results, we call for more defect characterization study in $ZnGeP_2$ using experimental techniques besides PL and EPR, and propose that the passivation of antisite defects and lowering of crystal growth temperature should be necessary for developing high-power $ZnGeP_2$-based optical devices.

Acknowledgements

This work was supported by National Natural Science Foundation of China (NSFC) under grant Nos. 61722402 and 91833302, Shanghai Academic/Technology Research Leader (19XD1421300), the Program for Professor of Special Appointment (Eastern Scholar), Fok Ying Tung Education Foundation (161060) and the Fundamental Research Funds for the Central Universities.

References:

[1] T. H. Allik, S. Chandra, D. M. Rines, P. G. Schunemann, J. A. Hutchinson, and R. Utano, Tunable 7–12-μm optical parametric oscillator using a Cr,Er:YSGG laser to pump CdSe and $ZnGeP_2$ crystals, Opt. Lett. **22**, 597 (1997).

[2] P. B. Phua, K. S. Lai, R. F. Wu, and T. C. Chong, High-efficiency mid-infrared $ZnGeP_2$ optical parametric oscillator in a multimode-pumped tandem optical parametric oscillator, Appl. Opt. **38**, 563 (1999).

[3] K. L. Vodopyanov, F. Ganikhanov, J. P. Maffetone, I. Zwieback, and W. Ruderman, $ZnGeP_2$ optical parametric oscillator with 3.8–12.4-μm tunability, Opt. Lett. **25**, 841 (2000).

[4] S. Das, G. C. Bhar, S. Gangopadhyay, and C. Ghosh, Linear and nonlinear optical properties of $ZnGeP_2$ crystal for infrared laser device applications: revisited, Appl. Opt. **42**, 4335 (2003).

[5] A. A. Ionin *et al.*, Mode-locked CO laser frequency doubling in $ZnGeP_2$ with 25% efficiency, Laser Phys. Lett. **8**, 723 (2011).

[6] M. W. Haakestad, H. Fonnum, and E. Lippert, Mid-infrared source with 0.2 J pulse energy based on nonlinear conversion of Q-switched pulses in $ZnGeP_2$, Opt. Express **22**, 8556 (2014).

[7] M. Gebhardt, C. Gaida, P. Kadwani, A. Sincore, N. Gehlich, C. Jeon, L. Shah, and M. Richardson, High peak-power mid-infrared $ZnGeP_2$ optical parametric oscillator pumped by a Tm:fiber master oscillator power amplifier system, Opt. Lett. **39**, 1212 (2014).

[8] Z. Lei, C. Zhu, C. Xu, B. Yao, and C. Yang, Growth of crack-free $ZnGeP_2$ large single crystals for high-power mid-infrared OPO applications, J. Cryst. Growth **389**, 23 (2014).

[9] B. Q. Yao, Y. J. Shen, X. M. Duan, T. Y. Dai, Y. L. Ju, and Y. Z. Wang, A 41-W $ZnGeP_2$ optical parametric oscillator pumped by a Q-switched Ho:YAG laser, Opt. Lett. **39**, 6589 (2014).

[10] S. Wandel, M.-W. Lin, Y. Yin, G. Xu, and I. Jovanovic, Parametric generation and characterization of femtosecond mid-infrared pulses in $ZnGeP_2$, Opt. Express **24**, 5287 (2016).

[11] T. Kanai *et al.*, Parametric amplification of 100 fs mid-infrared pulses in $ZnGeP_2$ driven by a

Ho:YAG chirped-pulse amplifier, Opt. Lett. **42**, 683 (2017).
[12] M. Schellhorn, G. Spindler, and M. Eichhorn, Improvement of the beam quality of a high-pulse-energy mid-infrared fractional-image-rotation-enhancement $ZnGeP_2$ optical parametric oscillator, Opt. Lett. **42**, 1185 (2017).
[13] A. A. Ionin, O. Kinyaevskiy, Y. M. Klimachev, V. A. Mozhaev, and Y. M. Andreev, Three-stage frequency conversion o sub-microsecond multiline CO laser pulse in a single $ZnGeP_2$ crystal, Opt. Lett. **43**, 3184 (2018).
[14] C.-P. Qian, B.-Q. Yao, B.-R. Zhao, G.-Y. Liu, X.-M. Duan, T.-Y. Dai, Y.-L. Ju, and Y.-Z. Wang, High repetition rate 102□□W middle infrared $ZnGeP_2$ master oscillator power amplifier system with thermal lens compensation, Opt. Lett. **44**, 715 (2019).
[15] G.-Y. Liu, Y. Chen, B.-Q. Yao, R.-x. Wang, K. Yang, C. Yang, S.-y. Mi, T.-Y. Dai, and X.-M. Duan, 3.5□□W long-wave infrared $ZnGeP_2$ optical parametric oscillator at 9.8□□μm, Opt. Lett. **45**, 2347 (2020).
[16] S. Cheng, G. Chatterjee, F. Tellkamp, T. Lang, A. Ruehl, I. Hartl, and R. J. Dwayne Miller, Compact Ho:YLF-pumped $ZnGeP_2$-based optical parametric amplifiers tunable in the molecular fingerprint regime, Opt. Lett. **45**, 2255 (2020).
[17] S. D. Setzler, N. C. Giles, L. E. Halliburton, P. G. Schunemann, and T. M. Pollak, Electron paramagnetic resonance of a cation antisite defect in $ZnGeP_2$, Appl. Phys. Lett. **74**, 1218 (1999).
[18] S. D. Setzler, P. G. Schunemann, T. M. Pollak, M. C. Ohmer, J. T. Goldstein, F. K. Hopkins, K. T. Stevens, L. E. Halliburton, and N. C. Giles, Characterization of defect-related optical absorption in $ZnGeP_2$, J. Appl. Phys. **86**, 6677 (1999).
[19] N. Dietz, I. Tsveybak, W. Ruderman, G. Wood, and K. J. Bachmann, Native defect related optical properties of $ZnGeP_2$, Appl. Phys. Lett. **65**, 2759 (1994).
[20] L. Wang, L. Bai, K. T. Stevens, N. Y. Garces, N. C. Giles, S. D. Setzler, P. G. Schunemann, and T. M. Pollak, Luminescence associated with copper in $ZnGeP_2$, J. Appl. Phys. **92**, 77 (2002).
[21] N. C. Giles, L. Bai, M. M. Chirila, N. Y. Garces, K. T. Stevens, P. G. Schunemann, S. D. Setzler, and T. M. Pollak, Infrared absorption bands associated with native defects in $ZnGeP_2$, J. Appl. Phys. **93**, 8975 (2003).
[22] D. M. Hofmann, N. G. Romanov, W. Gehlhoff, D. Pfisterer, B. K. Meyer, D. Azamat, and A. Hoffmann, Optically detected magnetic resonance experiments on native defects in $ZnGeP_2$, Physica B **340-342**, 978 (2003).
[23] M. Moldovan, K. T. Stevens, L. E. Halliburton, P. G. Schunemann, T. M. Pollak, S. D. Setzler, and N. C. Giles, Photoluminescence and EPR of Phosphorus Vacancies in $ZnGeP_2$, MRS Proceedings **607**, 445, 445 (2011).
[24] Y. Yang, Y. Zhang, Q. Gu, H. Zhang, and X. Tao, Growth and annealing characterization of $ZnGeP_2$ crystal, J. Cryst. Growth **318**, 721 (2011).
[25] G. Zhang, X. Tao, S. Wang, G. Liu, Q. Shi, and M. Jiang, Growth and thermal annealing effect on infrared transmittance of $ZnGeP_2$ single crystal, J. Cryst. Growth **318**, 717 (2011).
[26] V. N. Brudnyi, D. L. Budnitskii, M. A. Krivov, R. V. Masagutova, V. D. Prochukhan, and Y. V. Rud, The electrical and optical properties of 2.0 MeV electron-irradiated $ZnGeP_2$, Phys. Status Solidi A **50**, 379 (1978).
[27] G. Balčaitis, Z. Januškevičius, and A. Sodeika, On the Nature of Energy Levels in $ZnGeP_2$, Phys. Status Solidi A **89**, K71 (1985).
[28] M. H. Rakowsky *et al.*, Electron paramagnetic resonance study of a native acceptor in as−grown

$ZnGeP_2$, Appl. Phys. Lett. **64**, 1615 (1994).
[29] X. Zhao, S. Zhu, B. Zhao, B. Chen, Z. He, R. Wang, H. Yang, Y. Sun, and J. Cheng, Growth and characterization of $ZnGeP_2$ single crystals by the modified Bridgman method, J. Cryst. Growth **311**, 190 (2008).
[30] S. Xia, M. Wang, C. Yang, Z. Lei, G. Zhu, and B. Yao, Vertical Bridgman growth and characterization of large $ZnGeP_2$ single crystals, J. Cryst. Growth **314**, 306 (2011).
[31] G. C. Xing, K. J. Bachmann, and J. B. Posthill, High−pressure vapor transport of $ZnGeP_2$, Appl. Phys. Lett. **56**, 271 (1990).
[32] G. K. Averkieva, V. S. Grigoreva, I. A. Maltseva, V. D. Prochukhan, and Y. V. Rud, Photoluminescence of p-type $ZnGeP_2$ crystals, Phys. Status Solidi A **39**, 453 (1977).
[33] G. A. Verozubova, A. I. Gribenyukov, M. C. Ohmer, N. C. Fernelius, and J. T. Goldstein, Growth and characterization of epitaxial films of $ZnGeP_2$, MRS Proceedings **744**, M8.46, M8.46 (2011).
[34] Q. Fan, S. Zhu, B. Zhao, B. Chen, Z. He, J. Cheng, and T. Xu, Influence of annealing on optical and electrical properties of $ZnGeP_2$ single crystals, J. Cryst. Growth **318**, 725 (2011).
[35] A. Hoffmann *et al.*, Native Defect Characterization in $ZnGeP_2$, MRS Proceedings **607**, 373, 373 (2000).
[36] M. Moldovan and N. C. Giles, Broad-band photoluminescence from $ZnGeP_2$, J. Appl. Phys. **87**, 7310 (2000).
[37] C. I. Rablau and N. C. Giles, Sharp-line luminescence and absorption in $ZnGeP_2$, J. Appl. Phys. **90**, 3314 (2001).
[38] X. Jiang, M. S. Miao, and W. R. L. Lambrecht, Theoretical study of the phosphorus vacancy in $ZnGeP_2$, Phys. Rev. B **73**, 193203 (2006).
[39] X. Jiang, M. S. Miao, and W. R. L. Lambrecht, Theoretical study of cation-related point defects in $ZnGeP_2$, Phys. Rev. B **71**, 205212 (2005).
[40] X. Jiang and W. R. L. Lambrecht, Jahn–Teller Distortion of the Zinc Vacancy in $ZnGeP_2$, Chinese Phys. Lett. **25**, 1075 (2008).
[41] X. Jiang and W. R. L. Lambrecht, The importance of the self-interaction correction for Jahn–Teller distortion of the zinc vacancy in $ZnGeP_2$, Solid State Commun. **149**, 685 (2009).
[42] N. Dietz, W. Busse, H. E. Gumlich, W. Ruderman, I. Tsveybak, G. Wood, and K. J. Bachmann, Defect Characterization in $ZnGeP_2$ by Time-Resolved Photoluminescence, MRS Proceedings **450**, 333, 333 (2011).
[43] N. C. Giles, L. E. Halliburton, P. G. Schunemann, and T. M. Pollak, Photoinduced electron paramagnetic resonance of the phosphorus vacancy in $ZnGeP_2$, Appl. Phys. Lett. **66**, 1758 (1995).
[44] W. Gehlhoff, D. Azamat, and A. Hoffmann, EPR studies of native and impurity-related defects in II–IV–V_2 semiconductors, Mater. Sci. Semicond. Process. **6**, 379 (2003).
[45] W. Gehlhoff and A. Hoffmann, EPR identification of intrinsic and transition metal-related defects in $ZnGeP_2$ and other II–IV–V_2 compounds, Physica B **404**, 4942 (2009).
[46] U. Kaufmann, J. Schneider, and A. Räuber, ESR detection of antisite lattice defects in GaP, $CdSiP_2$, and $ZnGeP_2$, Appl. Phys. Lett. **29**, 312 (1976).
[47] P. Zapol, R. Pandey, M. Ohmer, and J. Gale, Atomistic calculations of defects in $ZnGeP_2$, J. Appl. Phys. **79**, 671 (1996).
[48] V. N. Brudnyĭ, V. G. Voevodin, and S. N. Grinyaev, Deep levels of intrinsic point defects and the nature of “anomalous” optical absorption in $ZnGeP_2$, Phys. Solid State **48**, 2069 (2006).
[49] S. Chen, P. Narang, H. A. Atwater, and L.-W. Wang, Phase Stability and Defect Physics of a

Ternary ZnSnN2 Semiconductor: First Principles Insights, Adv. Mater. **26**, 311 (2014).
[50] N. Tsunoda, Y. Kumagai, A. Takahashi, and F. Oba, Electrically Benign Defect Behavior in Zinc Tin Nitride Revealed from First Principles, Phys. Rev. Appl. **10**, 011001 (2018).
[51] D. Skachkov, A. Punya Jaroenjittichai, L.-y. Huang, and W. R. L. Lambrecht, Native point defects and doping in $ZnGeN_2$, Phys. Rev. B **93**, 155202 (2016).
[52] N. L. Adamski, Z. Zhu, D. Wickramaratne, and C. G. Van de Walle, Hybrid functional study of native point defects and impurities in $ZnGeN_2$, J. Appl. Phys. **122**, 195701 (2017).
[53] Y. Kumagai, M. Choi, Y. Nose, and F. Oba, First-principles study of point defects in chalcopyrite $ZnSnP_2$, Phys. Rev. B **90**, 125202 (2014).
[54] X. Wu, F. Meng, D. Chu, M. Yao, K. Guan, D. Zhang, and J. Meng, Carrier Tuning in $ZnSnN_2$ by Forming Amorphous and Microcrystalline Phases, lnorg. Chem. **58**, 8480 (2019).
[55] S. Nakatsuka, N. Yuzawa, J. Chantana, T. Minemoto, and Y. Nose, Solar cells using bulk crystals of rare metal-free compound semiconductor $ZnSnP_2$, Phys. Status Solidi A **214**, 1600650 (2017).
[56] M. A. Ryan, M. W. Peterson, D. L. Williamson, J. S. Frey, G. E. Maciel, and B. A. Parkinson, Metal site disorder in zinc tin phosphide, J. Mater. Res. **2**, 528 (2011).
[57] G. Kresse and J. Hafner, Ab initio molecular dynamics for liquid metals, Phys. Rev. B **47**, 558 (1993).
[58] J. Heyd and G. E. Scuseria, Efficient hybrid density functional calculations in solids: Assessment of the Heyd–Scuseria–Ernzerhof screened Coulomb hybrid functional, J. Chem. Phys. **121**, 1187 (2004).
[59] J. Heyd, J. E. Peralta, G. E. Scuseria, and R. L. Martin, Energy band gaps and lattice parameters evaluated with the Heyd-Scuseria-Ernzerhof screened hybrid functional, J. Chem. Phys. **123**, 174101 (2005).
[60] G. Kresse and D. Joubert, From ultrasoft pseudopotentials to the projector augmented-wave method, Phys. Rev. B **59**, 1758 (1999).
[61] P. E. Blöchl, Projector augmented-wave method, Phys. Rev. B **50**, 17953 (1994).
[62] H. J. Monkhorst and J. D. Pack, Special points for Brillouin-zone integrations, Phys. Rev. B **13**, 5188 (1976).
[63] C. G. Van de Walle and J. Neugebauer, First-principles calculations for defects and impurities: Applications to III-nitrides, J. Appl. Phys. **95**, 3851 (2004).
[64] C. Freysoldt, B. Grabowski, T. Hickel, J. Neugebauer, G. Kresse, A. Janotti, and C. G. Van de Walle, First-principles calculations for point defects in solids, Rev. Mod. Phys. **86**, 253 (2014).
[65] G. Makov and M. C. Payne, Periodic boundary conditions in ab initio calculations, Phys. Rev. B **51**, 4014 (1995).
[66] S. Lany and A. Zunger, Assessment of correction methods for the band-gap problem and for finite-size effects in supercell defect calculations: Case studies for ZnO and GaAs, Phys. Rev. B **78**, 235104 (2008).
[67] J. Ma, S.-H. Wei, T. A. Gessert, and K. K. Chin, Carrier density and compensation in semiconductors with multiple dopants and multiple transition energy levels: Case of Cu impurities in CdTe, Phys. Rev. B **83**, 245207 (2011).
[68] J.-H. Yang, J.-S. Park, J. Kang, W. Metzger, T. Barnes, and S.-H. Wei, Tuning the Fermi level beyond the equilibrium doping limit through quenching: The case of CdTe, Phys. Rev. B **90**, 245202 (2014).
[69] X. Yan, P. Li, L. Kang, S.-H. Wei, and B. Huang, First-principles study of electronic and diffusion

properties of intrinsic defects in 4H-SiC, J. Appl. Phys. **127**, 085702 (2020).
[70] S. Chen, A. Walsh, X.-G. Gong, and S.-H. Wei, Classification of Lattice Defects in the Kesterite $Cu_2ZnSnS4$ and $Cu2ZnSnSe_4$ Earth-Abundant Solar Cell Absorbers, Adv. Mater. **25**, 1522 (2013).
[71] F. Schanovsky, W. Gös, and T. Grasser, Multiphonon hole trapping from first principles, J. Vac. Sci. Technol. B **29**, 01A201 (2011).
[72] A. Alkauskas, J. L. Lyons, D. Steiauf, and C. G. Van de Walle, First-Principles Calculations of Luminescence Spectrum Line Shapes for Defects in Semiconductors: The Example of GaN and ZnO, Phys. Rev. Lett. **109**, 267401 (2012).
[73] B. P. Zapol, New expressions for the overlap integral of two linear harmonic oscillator wavefunctions, Chem. Phys. Lett. **93**, 549 (1982).
[74] J. P. Perdew, K. Burke, and M. Ernzerhof, Generalized Gradient Approximation Made Simple, Phys. Rev. Lett. **77**, 3865 (1996).
[75] D. M. Ceperley and B. J. Alder, Ground State of the Electron Gas by a Stochastic Method, Phys. Rev. Lett. **45**, 566 (1980).
[76] R. Bendorius, V. D. Prochukhan, and A. Šileika, The Lowest Conduction Band Minima of A^2B^4C-Type Semiconductors, Phys. Status Solidi B **53**, 745 (1972).
[77] M. C. Petcu, N. C. Giles, P. G. Schunemann, and T. M. Pollak, Band-Edge Photoluminescence at Room Temperature from $ZnGeP_2$ and $AgGaSe_2$, Phys. Status Solidi B **198**, 881 (1996).
[78] B. Zhang, X. Zhang, J. Yu, Y. Wang, K. Wu, and M.-H. Lee, First-Principles High-Throughput Screening Pipeline for Nonlinear Optical Materials: Application to Borates, Chem. Mat. **32**, 6772 (2020).
[79] B. R. Pamplin, T. Kiyosawa, and K. Masumoto, Ternary chalcopyrite compounds, Prog. Cryst. Growth Ch. **1**, 331 (1979).
[80] K. V. Shportko, Optical phonon behaviors in $ZnGeP_2$ single crystals from temperature dependent far-infrared reflectance spectra, Vib. Spectrosc **80**, 1 (2015).
[81] A. V. Krivosheeva, V. L. Shaposhnikov, V. V. Lyskouski, V. E. Borisenko, F. A. d'Avitaya, and J. L. Lazzari, Prospects on Mn-doped $ZnGeP_2$ for spintronics, Microelectron Reliab **46**, 1747 (2006).
[82] S. Limpijumnong, W. R. L. Lambrecht, and B. Segall, Electronic structure of $ZnGeP_2$: A detailed study of the band structure near the fundamental gap and its associated parameters, Phys. Rev. B **60**, 8087 (1999).
[83] R. Cao, H.-X. Deng, J.-W. Luo, and S.-H. Wei, Origin of the anomalous trends in band alignment of $GaX/ZnGeX_2$ (X = N, P, As, Sb) heterojunctions, J. Semicond. **40**, 042102 (2019).
[84] S.-R. Zhang, S.-F. Zhu, L.-H. Xie, X.-W. Chen, and K.-H. Song, Theoretical study of the structural, elastic and thermodynamic properties of chalcopyrite $ZnGeP_2$, Mater. Sci. Semicond. Process. **38**, 41 (2015).
[85] D. Yang, B. Zhao, B. Chen, S. Zhu, Z. He, W. Huang, Z. Zhao, and M. Liu, Impurity phases analysis of $ZnGeP_2$ single crystal grown by Bridgman method, J. Alloys Compd. **709**, 125 (2017).
[86] S. B. Zhang and J. E. Northrup, Chemical potential dependence of defect formation energies in GaAs: Application to Ga self-diffusion, Phys. Rev. Lett. **67**, 2339 (1991).
[87] J. L. Lyons and C. G. Van de Walle, Computationally predicted energies and properties of defects in GaN, NPJ Comput. Mater. **3**, 12 (2017).
[88] A. P. Seitsonen, R. Virkkunen, M. J. Puska, and R. M. Nieminen, Indium and phosphorus vacancies and antisites in InP, Phys. Rev. B **49**, 5253 (1994).
[89] A. Janotti and C. G. Van de Walle, Native point defects in ZnO, Phys. Rev. B **76**, 165202 (2007).